Title

Mapping Buried Hydrogen-Bonding Networks

Journal

ACS Nano, 10(5)

ISSN

1936-0851

Authors

Thomas, John C

Goronzy, Dominic P

Dragomiretskiy, Konstantin

et al.

Publication Date

2016-05-24

DOI

10.1021/acsnano.6b01717

Peer reviewed

ACSNANO
www.acsnano.org
ARTICLE

Mapping Buried Hydrogen-Bonding Networks

John C. Thomas,[†,‡] Dominic P. Goronzy,[†,‡] Konstantin Dragomiretskiy,[‡,§] Dominique Zosso,[‡,§] Jérôme Gilles,[∥] Stanley J. Osher,[*,§] Andrea L. Bertozzi,[*,§] and Paul S. Weiss[*,†,‡,⊥]

[†]Department of Chemistry and Biochemistry, University of California, Los Angeles, Los Angeles, California 90095, United States
[‡]California NanoSystems Institute, University of California, Los Angeles, Los Angeles, California 90095, United States
[§]Department of Mathematics, University of California, Los Angeles, Los Angeles, California 90095, United States
[∥]Department of Mathematics and Statistics, San Diego State University, San Diego, California 92182, United States
[⊥]Department of Materials Science and Engineering, University of California, Los Angeles, Los Angeles, California 90095, United States

Supporting Information

ABSTRACT: **We map buried hydrogen-bonding networks within self-assembled monolayers of 3-mercapto-*N*-nonylpropionamide on Au{111}. The contributing interactions include the buried S−Au bonds at the substrate surface and the buried plane of linear networks of hydrogen bonds. Both are simultaneously mapped with submolecular resolution, in addition to the exposed interface, to determine the orientations of molecular segments and directional bonding. Two-dimensional mode-decomposition techniques are used to elucidate the directionality of these networks. We find that amide-based hydrogen bonds cross molecular domain boundaries and areas of local disorder.**

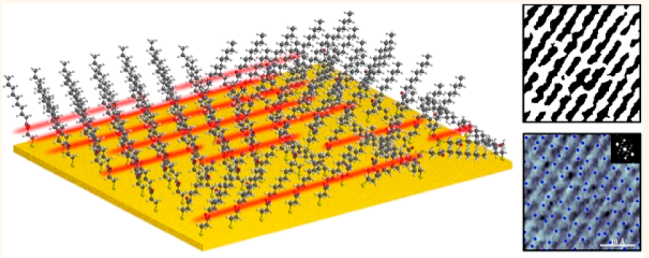

KEYWORDS: *self-assembly, hydrogen bonding, scanning tunneling microscopy, image analysis, two-dimensional variational mode decomposition, segmentation, spectroscopic imaging, self-assembled monolayers, disorder*

Nanotechnology is intrinsically dependent upon the interactions between molecules, where bottom-up assembly aims to control single chemical units, linear arrays, two-dimensional thin films, and three-dimensional architectures by tuning and controlling chemical interactions at all scales. Self-assembled monolayers (SAMs), where surfactants spontaneously form in order on substrates, enable the placement and direction of single molecules and supramolecular assemblies on surfaces.[1−4] Monolayers can be tuned through a variety of different interactions, where designing and tuning intermolecular interactions become pathways to create robust, adjustable, and even precise formations. To this end, self-assembly has found use in molecular coatings, substrate electronic property modification, processable biosensors, and other areas.[5−7] Scanning tunneling microscopy (STM) is able to record and to leverage sparse details, in that single-component information can be differentiated and compared to ensemble measurements and individual molecules and features are often oversampled. Prompted by the analytical power and resolution of STM, a number of efforts have focused on developing multimodal spectroscopic imaging capabilities.[8−15]

Monolayers composed of 3-mercapto-*N*-nonylpropionamide (1ATC9) have been extensively studied; however, the buried hydrogen-bonding network presumed responsible for the stability and directionality of these systems has not previously been visualized.[16−23] Indeed, it has been a long-standing challenge to measure buried chemical functionality with molecular and submolecular resolution.[10,15,24−29] Using 1ATC9 monolayers as a model system, we have measured buried hydrogen-bonding networks within (single-component amide-containing) SAMs and visualized bonding and interactions previously hidden from conventional scanning probe techniques.

Many single-molecule techniques remain hindered by either extreme dilution or lack of specificity, whereas STM is able to resolve chemical state information at the single-molecule and atomic levels.[10,22,24−27,30,31] Rastering an atomically sharp tip across a conductive substrate enables the acquisition of apparent height information, where the measured data are convolutions of electronic and topographic structure. In the case of SAMs, where the probe tip does not penetrate the film, the exposed surface is measured.[28] Upon applying an AC modulation to the tunneling-gap distance, the local surface work function can be accessed with sub-angström precision.[29,32,33] This technique has been previously employed to measure the tilt of dual component alkanethiolate monolayers,

Received: March 10, 2016
Accepted: April 20, 2016
Published: April 20, 2016

DOI: 10.1021/acsnano.6b01717
ACS Nano 2016, 10, 5446−5451

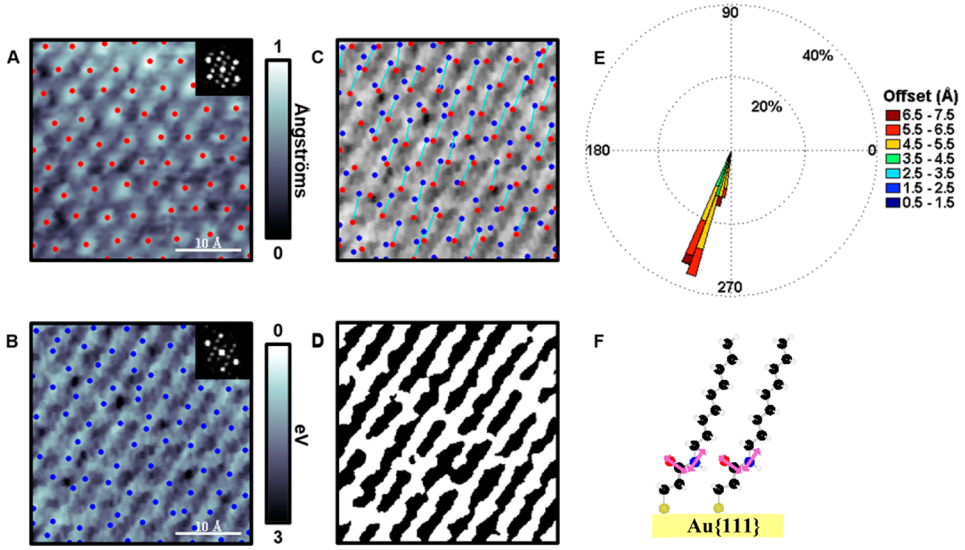

Figure 1. (A) Scanning tunneling microscope topographic image ($I_{tunneling}$ = 15 pA, V_{sample} = −0.5 V) and (B) simultaneously acquired local barrier height (LBH) map over an area of the more tilted (18°) structure of 3-mercapto-*N*-nonylpropionamide (1ATC9), with respect to the underlying Au{111} surface. The local maxima of both topography (red) and inverted LBH (blue) in B are computed. Insets depict fast Fourier transforms showing the expected topographic hexagonal nearest-neighbor spacing, which is also found within LBH images. (C) All maxima were connected within a defined radial range and orientation; best fit molecular orientations show the expected polar tilt angles. (D) Thresholded image binary of B, which highlights the 1D linear networks of hydrogen bonds. (E) Rose plot (depicting fitted maximum offsets) binned by both magnitude (0.5 Å bins) and orientation (4° bins). (F) A ball-and-stick model of 1ATC9 showing a polar chain tilt of 18° (for the molecular segment above the amide) and amide bonds nearly parallel to the substrate.

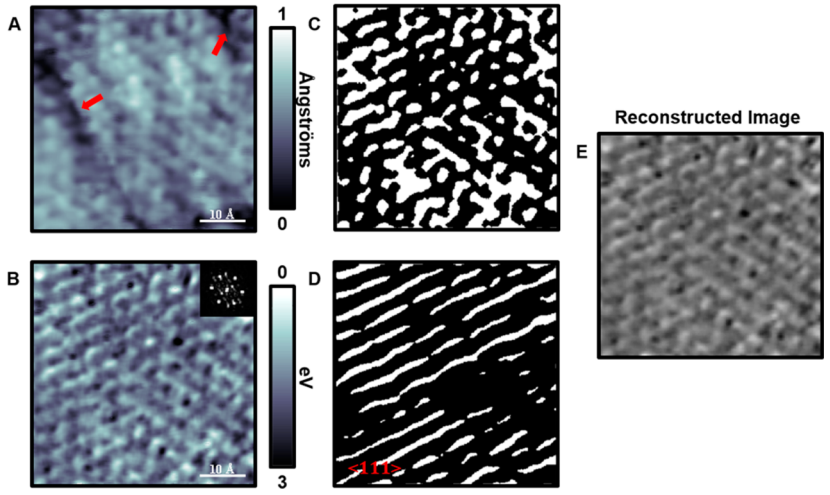

Figure 2. (A) Scanning tunneling micrograph ($I_{tunneling}$ = 15 pA, V_{sample} = −0.5 V) of three domains of a self-assembled monolayer of 3-mercapto-*N*-nonylpropionamide (1ATC9), where a lattice registry offset domain and an area of topographic disorder are highlighted by red arrows. (B) Simultaneously acquired local barrier height map of the same area measured in A. The inset depicts a fast Fourier transform of B, which is used for image decomposition. (C) Thresholded image binary of B. (D) Results obtained by two-dimensional variational mode decomposition of the ⟨111⟩ directional mode, where amide bonds cross each topographic domain highlighted in A, and a buried region of local disorder is depicted in the middle-right part of the image. (E) Reconstructed image of all deconstructed modes that tests the employed methodology (see Supplemental Figure S2 for all deconstructed modes).

where local extrema were related to the largest buried dipole (Au−S bond).[28] In carboranethiolate (symmetric cage molecules) self-assembled monolayers, topographic and local barrier height modalities were correlated to reveal single-molecule orientations and dipolar alignment within homogeneous monolayers.[29] Motivated by these recent technical advances in imaging and image analysis, we sought to resolve individual hydrogen bonds and the subsequently formed buried networks within monolayers of 1ATC9.

Amide and hydrogen bonds are of fundamental importance to molecular structure and biological function.[34−39] The precise interplay between single- and supramolecular constructs and biochemical function remains one of the elusive and quintessential aspects of biology. Charge separation within the amide bond has been extensively studied and shown to vary with different chemical substituents, leading to (hydrogen-) bonding enthalpies ranging from 2 to 65 kcal/mol, but typically much stronger than van der Waals interactions (~5 kcal/mol)[35] and can be comparable to the Au−S bond (~50 kcal/mol) and

DOI: 10.1021/acsnano.6b01717
ACS Nano 2016, 10, 5446−5451

Au−Au bonds (~44 kcal/mol).[40] The dipole moment for amide bonds (~3.7 D) is larger than that for Au−S bonds (1−2 D)[41,42] and helps to explain why different tilt orientations, in monolayers composed of 1ATC9, reflect orientations of the amide dipoles.[4] In terms of molecular self-assembly, the presence of amide groups within monolayers composed of 1ATC9 enables increases in intermolecular interactions between nearest neighbors and leads to the formation of stable, protective ultrathin coatings that have been shown to prevent oxidation of liquid-metal nanoparticles.[43] Electrochemical measurements, performed by Clegg *et al.*, indicated that electron transfer was indeed kinetically limited, providing evidence that neither analyte permeation nor analyte pinhole diffusion played a significant role and thus electron transfer was primarily due to electronic coupling between chains. Infrared spectroscopy measurements also showed that amide-containing SAMs of varied chain length were extensively ordered with C═O and N−H bonds nearly parallel to the substrate plane.[18] We used buried amide-based hydrogen-bonding networks to encapsulate liquid-metal nanoparticles and to prevent oxidation.[43] With significant ensemble evidence of buried networks, it becomes increasingly important and feasible to *map* the networks within these systems directly.

RESULTS AND DISCUSSION

The two tilt phases of 1ATC9 can be conventionally distinguished by apparent height using STM in topographic mode; however, scanning tunneling spectroscopy (STS) is able to access *both* topographic and buried information in local barrier height mode to enable a more precise structural identification.[28,29] We use a custom-built scanning tunneling microscope held at low temperature (4 K) and extreme high vacuum ($\leq 10^{-12}$ Torr) for this purpose.[44] Topographic images depict the expected $(\sqrt{3} \times \sqrt{3})R30°$ superstructure; however, we observe contrast reversal, under these conditions, in comparison to measurements recorded at room temperature.[19,23] This reversal is consistent with stronger electronic influences, rather than topographic features, which have also been reported in STM images of peptide assemblies.[34] Images show a distinct structural dependence in local barrier height (LBH) mode, where the tilted structure (18°) (Figures 1 and 2), with respect to the underlying substrate normal, shows local barrier height contrast differences compared to the normally oriented (0°) structure and can be segmented by conventional image thresholding (Figure 3). The ability to distinguish each structure *via* LBH imaging permits segmentation and the relative determination of individual alkyl chain segment tilts and orientations within molecules. We controllably assembled our samples to form predominantly the 18° structure through high-temperature annealing, as determined by Kim *et al.* previously, but can still measure small areas of the 0° structure.[23]

We have previously measured the polar and azimuthal tilt angles of the saturated chains of *n*-alkanethiols self-assembled on Au{111}.[28] We use these prior measurements, of one buried dipole per molecule, due to the S−Au bond, as control experiments for the measurements and analyses described here.

Analyses within areas composed of the 18° tilt structure are able to retrieve both molecular tilts, compared with previous ensemble results, and one-dimensional (1D) hydrogen-bonding networks, as shown in Figure 1. To determine tilts and solid angles, we measured all distances within a defined radial range and computed lateral offsets, azimuthal orientations, and tilts,

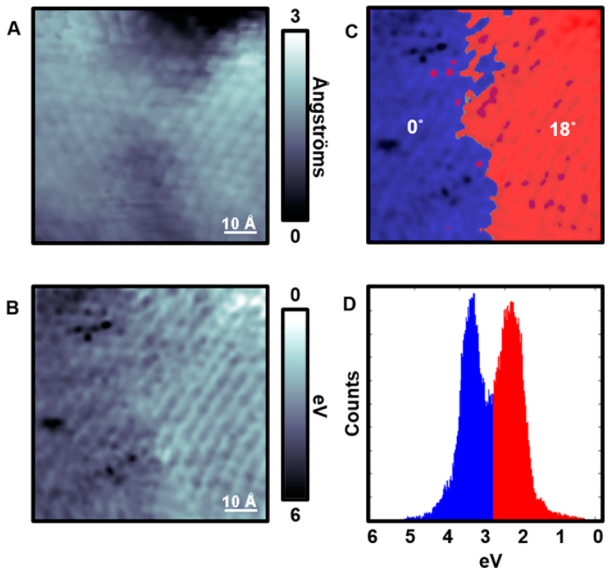

Figure 3. (A) Scanning tunneling micrograph of 3-mercapto-*N*-nonylpropionamide on Au{111} along a tilt domain ($I_{tunneling}$ = 15 pA, V_{sample} = −0.5 V). (B) Simultaneously acquired local barrier height (LBH) image of A. (C) We separate the upper (highlighted as red) and lower (highlighted as blue) domains in LBH based on relative work function differences. (D) Image histogram of C showing the energy cutoff used that was also fit with two Gaussian curves to solve for peak-to-peak image contrast differences.

with respect to the surface normal. This information and the directional criteria used are presented in Table S1, where the polar angles determined are consistent, within experimental error, with previous structural analyses.[16,23] Little prior information, however, has been available on azimuthal orientations. Applying a threshold to LBH images to form an image binary highlights the 1D orientations of hydrogen bonds, where the LBH data obtained contain contributions from both the buried Au−S and amide dipoles. Here, 1D variations may be attributed to local differences in amide bond orientation, which are predominantly in one direction. These buried domains span areas of tens to hundreds of nanometers, and cross structural domains and disordered regions, as measured *via* topographic imaging (Figure 2). We compare analyses obtained by two-dimensional variational mode decomposition (2DVMD) to straightforward thresholded images (Figure S1). Variational mode decomposition builds upon empirical mode decomposition, which is used to detect and to decompose images into principal modes, with nonrecursive methods that are fully adaptive.[45,46] A mode, in this context, is based on an intrinsic mode function that meets two conditions: the number of extrema and the number of zero crossings differ at most by one, and the mean values of the local maxima and local minima envelopes are zero.[47] The thresholded image binary retains all principal modes, where 2DVMD succeeds in decomposing each mode into different crystalline directions and enables full image reconstruction. We show all principal modes (Figure S2) obtained that are, again, verified by summing each mode into the reconstructed, original signal shown in Figure 2B. The ⟨111⟩ direction is emphasized, which distinguishes a buried region of disorder that is underrepresented, where the same area is strongly represented in the $\langle 11\bar{1} \rangle$ direction. Thus, we are able to determine that hydrogen bonds cross the topographic domains featured in Figure 2A.

DOI: 10.1021/acsnano.6b01717
ACS Nano 2016, 10, 5446−5451

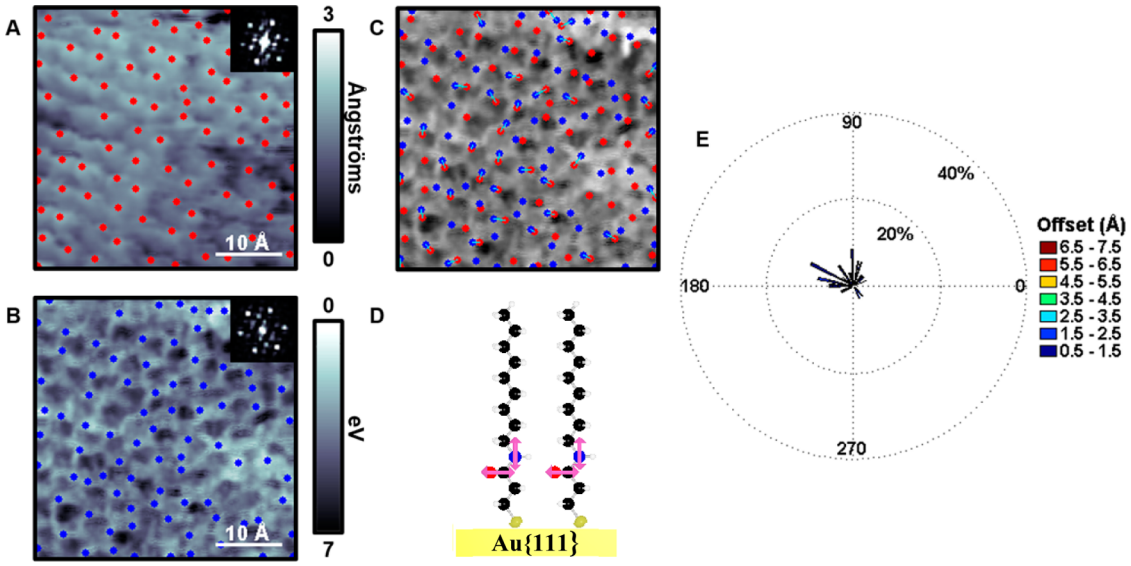

Figure 4. (A) Scanning tunneling microscope topographic image ($I_{tunneling}$ = 15 pA, V_{sample} = −0.5 V) and (B) simultaneously acquired local barrier height (LBH) map over the normally oriented (0°) structure, with respect to the underlying Au{111} substrate, within monolayers of 3-mercapto-*N*-nonylpropionamide (1ATC9). Local maxima in both topography (red) in A and inverted LBH (blue) in B are computed. Insets depict fast Fourier transforms of both topography and LBH images. (C) Computed molecular orientations overlaid onto the LBH map. (D) A ball-and-stick model of 1ATC9 normally oriented on a Au substrate. (E) Rose plot of measured vector orientations binned by both magnitude (0.5 Å bins) and orientation (4° bins), which indicates that the molecules are oriented near normal.

In the normally oriented phase, we used a block-matching approach to compare molecular apexes with dipolar extrema, where image patches (the size of one molecule) are correlated within larger LBH image patches (the size of nearest and next-nearest neighbors) to compute molecular orientations and the polar and azimuthal tilt angles of the *segments* of the molecular chains on each side of the amide functionality.[29,48,49] A randomly oriented lateral distance of 1.3 ± 0.4 Å was recorded that represents a near normal tilt (Figure 4), where nanoscale fluctuations can be understood by increased amide−amide interactions and an imperfect backbone structure formed after assembly.[18] We also measured all possible maxima offsets within a given radius and orientation (Table S2), where correlation yields the largest number of vector offsets. We have successfully measured the local landscape of both the buried Au−S bonds and the buried hydrogen-bonding networks using STM coupled with spectroscopic imaging.

CONCLUSIONS AND PROSPECTS

Our measurements have uncovered long-range networks between amide-containing SAM units and provide a new avenue to monitor and to characterize buried functionality within 2D matrices. Correlations and comparative analyses reveal both the hydrogen-bonding networks and the molecular orientations (tilts) of parts of each 1ATC9 molecule. As hydrogen bonding is critical in biomolecular and supramolecular assembly, we foresee broad and widespread applicability of elucidating important structures and interactions with this method.[4,34,38]

In retrospect, the robust, resilient hydrogen-bonding networks observed here are consistent with and help explain the protection (relative to oxidation) of the liquid-metal gallium−indium eutectic nanoparticles that we prepared *via* ultrasonication.[43] Likewise, buried hydrogen bonds have been used to stabilize the various states of molecular switches isolated in two-dimensional matrices;[22] the extended hydrogen-bonding networks discovered here would result in increased rigidity of the matrices and stability of the molecular switches relative to short-range interactions only. We have previously used switchable *exposed* hydrogen-bonding networks as protective layers in chemical patterning and nanolithography using SAMs.[50] In a more recently developed nanolithographic method, chemical lift-off lithography,[28,51] buried hydrogen-bonding layers should lead to more robust, rigid lifted-off metal monolayer structures.

Scanning tunneling microscopy is capable of resolving exquisite single-component chemical state information beyond ensemble structures.[13,29,52,53] Networks of buried hydrogen bonds have been resolved and span areas of tens to hundreds of square nanometers, crossing structural domain boundaries and regions of disorder.

MATERIALS AND METHODS

Scanning Tunneling Microscope Sample Preparation. The chemicals 3-mercapto-*N*-nonylpropionamide and neat benzene (Sigma-Aldrich, St. Louis, MO) were used as received. The Au{111} on mica substrates (Agilent Technology, Tempe, AZ) were hydrogen-flame-annealed prior to SAM formation with 10 passes at a rate of 0.4 Hz. Substrates were immersed into 1 mM solutions in benzene and held at 70 °C for 24 h. Each sample was removed from solution and cleaned by three cycles of rinsing with neat benzene and blown dry with nitrogen gas. The samples were immediately placed into the vacuum chamber, and lowered into the STM in the cryostat after sufficient vacuum was reached.

Imaging. All STM measurements were performed with an ultrastable, extreme high vacuum, low-temperature (10^{-12} Torr, 4 K) custom beetle-style STM with a platinum/iridium tip (80:20).[44] The known atomic spacing of Au{111} was used to calibrate all piezoelectric scanners. The sample was held at a fixed bias (V_{sample} = −0.5 V), and both topographic and LBH modalities were measured with constant-current feedback (I_t = 15 pA) at 256 × 256 pixel resolution. The tunneling gap distance was modulated at a frequency about the STM feedback loop bandwidth (~3 kHz) with a sinusoidal amplitude (dz ~0.1 Å), and d*I*/d*z* was recorded with a lock-in amplifier (Stanford Research Systems SR850 DSP, Sunnyvale, CA).

DOI: 10.1021/acsnano.6b01717
ACS Nano 2016, 10, 5446−5451

Local barrier height images were calibrated against a Au step edge, under the caveat that the LBH magnitude may vary in cases where the applied voltage may not always equal the voltage across the tunneling junction.[29,31]

Image Analyses. All STM images were initially processed with automated routines developed in MATLAB (Mathworks, Natick, MA) to remove any high-frequency noise and intensity spikes that may otherwise impair reliable segmentation.[28,29] Local barrier height images were inverted to highlight Au−S positions. We define local maxima in topographic $[p]$ and LBH images $[q]$ if its intensity was greater than that of all surrounding pixels within a molecular-sized window. For the normally oriented (0°) phase, each set of local maxima was obtained for both simultaneously acquired images, and a topographic image patch centered at each maxima point was correlated at each pixel against a larger LBH image patch, the size of one molecule and nearest-neighbor spacing, respectively. The maximum correlation was chosen for each maxima point, which was then referenced and plotted.[29,48,49] Image thresholds and masks were obtained with known processes in MATLAB. For the tilted (18°) phase, all maxima $[p\ q]$ were connected within a defined radial range and orientation, and then referenced and tabulated. Variational mode decomposition results were obtained with previously published MATLAB script.[45,46] Local barrier height image histograms shown in Figure 3 were fit against two Gaussian curves, and the peak-to-peak energy distance was referenced and reported.

ASSOCIATED CONTENT

Supporting Information

The Supporting Information is available free of charge on the ACS Publications website at DOI: 10.1021/acsnano.6b01717.

Data and figures that describe the image thresholding methodology, complete variational mode decomposition results, and tabulated values of all possible tilt orientations (within nearest-neighbor spacings) of the normally oriented phase (PDF)

AUTHOR INFORMATION

Corresponding Authors

*E-mail: psw@cnsi.ucla.edu (P.S.W.).
*E-mail: sjo@math.ucla.edu (S.J.O.).
*E-mail: bertozzi@math.ucla.edu (A.L.B.).

Notes

The authors declare no competing financial interest.

ACKNOWLEDGMENTS

The authors acknowledge support from the Department of Energy Grant No. DE-SC-0005025 for the experiments conducted and imaging methods developed and applied and from the W. M. Keck Foundation for the analytical methods developed and applied. J.C.T. acknowledges support from an Excellence in Chemistry Graduate Research Fellowship from UCLA. We gratefully thank H. Chong, Prof. S. A. Claridge, M. Gethers, A. I. Guttentag, Dr. J. N. Hohman, D. McMillan, M. A. Silverman, J. M. Abendroth, and L. A. Stewart for their advice and helpful discussions.

REFERENCES

(1) Ulman, A. Formation and Structure of Self-Assembled Monolayers. *Chem. Rev.* **1996**, *96*, 1533−1554.

(2) Love, J. C.; Estroff, L. A.; Kriebel, J. K.; Nuzzo, R. G.; Whitesides, G. M. Self-Assembled Monolayers of Thiolates on Metals as a Form of Nanotechnology. *Chem. Rev.* **2005**, *105*, 1103−1170.

(3) Weiss, P. S. Functional Molecules and Assemblies in Controlled Environments: Formation and Measurements. *Acc. Chem. Res.* **2008**, *41*, 1772−1781.

(4) Claridge, S. A.; Liao, W.-S.; Thomas, J. C.; Zhao, Y.; Cao, H. H.; Cheunkar, S.; Serino, A. C.; Andrews, A. M.; Weiss, P. S. From the Bottom Up: Dimensional Control and Characterization in Molecular Monolayers. *Chem. Soc. Rev.* **2013**, *42*, 2725−2745.

(5) Vericat, C.; Vela, M. E.; Benitez, G.; Carro, P.; Salvarezza, R. C. Self-Assembled Monolayers of Thiols and Dithiols on Gold: New Challenges for a Well-Known System. *Chem. Soc. Rev.* **2010**, *39*, 1805−1834.

(6) Kim, J.; Rim, Y. S.; Liu, Y.; Serino, A. C.; Thomas, J. C.; Chen, H.; Yang, Y.; Weiss, P. S. Interface Control in Organic Electronics Using Mixed Monolayers of Carboranethiol Isomers. *Nano Lett.* **2014**, *14*, 2946−2951.

(7) Kim, J.; Rim, Y. S.; Chen, H.; Cao, H. H.; Nakatsuka, N.; Hinton, H. L.; Zhao, C.; Andrews, A. M.; Yang, Y.; Weiss, P. S. Fabrication of High-Performance Ultrathin In_2O_3 Film Field-Effect Transistors and Biosensors Using Chemical Lift-Off Lithography. *ACS Nano* **2015**, *9*, 4572−4582.

(8) Berndt, R.; Gaisch, R.; Gimzewski, J. K.; Reihl, B.; Schlittler, R. R.; Schneider, W. D.; Tschudy, M. Photon Emission at Molecular Resolution Induced by a Scanning Tunneling Microscope. *Science* **1993**, *262*, 1425−1427.

(9) Stranick, S. J.; Weiss, P. S. Alternating Current Scanning Tunneling Microscopy and Nonlinear Spectroscopy. *J. Phys. Chem.* **1994**, *98*, 1762−1764.

(10) McCarty, G. S.; Weiss, P. S. Scanning Probe Studies of Single Nanostructures. *Chem. Rev.* **1999**, *99*, 1983−1990.

(11) Donhauser, Z. J.; Mantooth, B. A.; Kelly, K. F.; Bumm, L. A.; Monnell, J. D.; Stapleton, J. J.; Price, D. W., Jr.; Rawlett, A. M.; Allara, D. L.; Tour, J. M.; Weiss, P. S. Conductance Switching in Single Molecules through Conformational Changes. *Science* **2001**, *292*, 2303−2307.

(12) Wu, S. W.; Ogawa, N.; Ho, W. Atomic-Scale Coupling of Photons to Single-Molecule Junctions. *Science* **2006**, *312*, 1362−1365.

(13) Claridge, S. A.; Schwartz, J. J.; Weiss, P. S. Electrons, Photons, and Force: Quantitative Single-Molecule Measurements from Physics to Biology. *ACS Nano* **2011**, *5*, 693−729.

(14) Kim, M.; Hohman, J. N.; Cao, Y.; Houk, K. N.; Ma, H.; Jen, A. K.-Y.; Weiss, P. S. Creating Favorable Geometries for Directing Organic Photoreactions in Alkanethiolate Monolayers. *Science* **2011**, *331*, 1312−1315.

(15) Bonnell, D. A.; Basov, D. N.; Bode, M.; Diebold, U.; Kalinin, S. V.; Madhavan, V.; Novotny, L.; Salmeron, M.; Schwarz, U. D.; Weiss, P. S. Imaging Physical Phenomena with Local Probes: From Electrons to Photons. *Rev. Mod. Phys.* **2012**, *84*, 1343−1381.

(16) Tam-Chang, S.-W.; Biebuyck, H. A.; Whitesides, G. M.; Jeon, N.; Nuzzo, R. G. Self-Assembled Monolayers on Gold Generated from Alkanethiols with the Structure $RNHCOCH_2SH$. *Langmuir* **1995**, *11*, 4371−4382.

(17) Clegg, R. S.; Reed, S. M.; Hutchison, J. E. Self-Assembled Monolayers Stabilized by Three-Dimensional Networks of Hydrogen Bonds. *J. Am. Chem. Soc.* **1998**, *120*, 2486−2487.

(18) Clegg, R. S.; Hutchison, J. E. Control of Monolayer Assembly Structure by Hydrogen Bonding Rather Than by Adsorbate-Substrate Templating. *J. Am. Chem. Soc.* **1999**, *121*, 5319−5327.

(19) Lewis, P. A.; Smith, R. K.; Kelly, K. F.; Bumm, L. A.; Reed, S. M.; Clegg, R. S.; Gunderson, J. D.; Hutchison, J. E.; Weiss, P. S. The Role of Hydrogen Bonds in Self-Assembled Mixed Composition Thiols on Au{111}. *J. Phys. Chem. B* **2001**, *105*, 10630−10636.

(20) Smith, R. K.; Reed, S. M.; Lewis, P. A.; Monnell, J. D.; Clegg, R. S.; Kelly, K. F.; Bumm, L. A.; Hutchison, J. E.; Weiss, P. S. Phase Separation within a Binary Self-Assembled Monolayer on Au{111} Driven by an Amide-Containing Alkanethiol. *J. Phys. Chem. B* **2001**, *105*, 1119−1122.

(21) Lewis, P. A.; Inman, C. E.; Yao, Y.; Tour, J. M.; Hutchison, J. E.; Weiss, P. S. Mediating Stochastic Switching of Single Molecules Using Chemical Functionality. *J. Am. Chem. Soc.* **2004**, *126*, 12214−12215.

(22) Lewis, P. A.; Inman, C. E.; Maya, F.; Tour, J. M.; Hutchison, J. E.; Weiss, P. S. Molecular Engineering of the Polarity and Interactions

DOI: 10.1021/acsnano.6b01717
ACS Nano 2016, 10, 5446−5451

of Molecular Electronic Switches. *J. Am. Chem. Soc.* **2005**, *127*, 17421−17426.
(23) Kim, M.; Hohman, J. N.; Serino, A. C.; Weiss, P. S. Structural Manipulation of Hydrogen-Bonding Networks in Amide-Containing Alkanethiolate Monolayers *via* Electrochemical Processing. *J. Phys. Chem. C* **2010**, *114*, 19744−19751.
(24) Stipe, B. C.; Rezaei, M. A.; Ho, W. Single-Molecule Vibrational Spectroscopy and Microscopy. *Science* **1998**, *280*, 1732−1735.
(25) Lee, H. J.; Ho, W. Structural Determination by Single-Molecule Vibrational Spectroscopy and Microscopy: Contrast between Copper and Iron Carbonyls. *Phys. Rev. B: Condens. Matter Mater. Phys.* **2000**, *61*, R16347−R16350.
(26) Khuong, T.-A. V.; Nuñez, J. E.; Godinez, C. E.; Garcia-Garibay, M. A. Crystalline Molecular Machines: A Quest Toward Solid-State Dynamics and Function. *Acc. Chem. Res.* **2006**, *39*, 413−422.
(27) Michl, J.; Sykes, E. C. H. Molecular Rotors and Motors: Recent Advances and Future Challenges. *ACS Nano* **2009**, *3*, 1042−1048.
(28) Han, P.; Kurland, A. R.; Giordano, A. N.; Nanayakkara, S. U.; Blake, M. M.; Pochas, C. M.; Weiss, P. S. Heads and Tails: Simultaneous Exposed and Buried Interface Imaging of Monolayers. *ACS Nano* **2009**, *3*, 3115−3121.
(29) Thomas, J. C.; Schwartz, J. J.; Hohman, J. N.; Claridge, S. A.; Auluck, H. S.; Serino, A. C.; Spokoyny, A. M.; Tran, G.; Kelly, K. F.; Mirkin, C. A.; Gilles, J.; Osher, S. J.; Weiss, P. S. Defect-Tolerant Aligned Dipoles within Two-Dimensional Plastic Lattices. *ACS Nano* **2015**, *9*, 4734−4742.
(30) Han, P.; Akagi, K.; Canova, F. F.; Mutoh, H.; Shiraki, S.; Iwaya, K.; Weiss, P. S.; Asao, N.; Hitosugi, T. Bottom-Up Graphene-Nanoribbon Fabrication Reveals Chiral Edges and Enantioselectivity. *ACS Nano* **2014**, *8*, 9181−9187.
(31) Zhang, J.; Chen, P.; Yuan, B.; Ji, W.; Cheng, Z.; Qiu, X. Real-Space Identification of Intermolecular Bonding with Atomic Force Microscopy. *Science* **2013**, *342*, 611−614.
(32) Lang, N. D. Apparent Height in Scanning Tunneling Microscopy. *Phys. Rev. B: Condens. Matter Mater. Phys.* **1988**, *37*, 10395−10398.
(33) Monnell, J. D.; Stapleton, J. J.; Dirk, S. M.; Reinerth, W. A.; Tour, J. M.; Allara, D. L.; Weiss, P. S. Relative Conductances of Alkaneselenolate and Alkanethiolate Monolayers on Au{111}. *J. Phys. Chem. B* **2005**, *109*, 20343−20349.
(34) Claridge, S. A.; Thomas, J. C.; Silverman, M. A.; Schwartz, J. J.; Yang, Y.; Wang, C.; Weiss, P. S. Differentiating Amino Acid Residues and Side Chain Orientations in Peptides Using Scanning Tunneling Microscopy. *J. Am. Chem. Soc.* **2013**, *135*, 18528−18535.
(35) Glowacki, E. D.; Irimia-Vladu, M.; Bauer, S.; Sariciftci, N. S. Hydrogen-Bonds in Molecular Solids-From Biological Systems to Organic Electronics. *J. Mater. Chem. B* **2013**, *1*, 3742−3753.
(36) Harder, M.; Kuhn, B.; Diederich, F. Efficient Stacking on Protein Amide Fragments. *ChemMedChem* **2013**, *8*, 397−404.
(37) Fischer, F. R.; Wood, P. A.; Allen, F. H.; Diederich, F. Orthogonal Dipolar Interactions between Amide Carbonyl Groups. *Proc. Natl. Acad. Sci. U. S. A.* **2008**, *105*, 17290−17294.
(38) Etter, M. C. Encoding and Decoding Hydrogen-Bond Patterns of Organic Compounds. *Acc. Chem. Res.* **1990**, *23*, 120−126.
(39) Steiner, T. The Hydrogen Bond in the Solid State. *Angew. Chem., Int. Ed.* **2002**, *41*, 48−76.
(40) Liao, W.-S.; Cheunkar, S.; Cao, H. H.; Bednar, H. R.; Weiss, P. S.; Andrews, A. A. Subtractive Patterning *via* Chemical Lift-Off Lithography. *Science* **2012**, *337*, 1517−1521.
(41) Meighan, R. M.; Cole, R. H. Dielectric Properties of Alkyl Amides. I. Vapor Phase Dipole Moments and Polarization in Benzene Solution. *J. Phys. Chem.* **1964**, *68*, 503−508.
(42) Sellers, H.; Ulman, A.; Shnidman, Y.; Eilers, J. E. Structure and Binding of Alkanethiolates on Gold and Silver Surfaces: Implications for Self-Assembled Monolayers. *J. Am. Chem. Soc.* **1993**, *115*, 9389−9401.
(43) Hohman, J. N.; Kim, M.; Wadsworth, G. A.; Bednar, H. R.; Jiang, J.; LeThai, M. A.; Weiss, P. S. Directing Substrate Morphology *via* Self-Assembly: Ligand-Mediated Scission of Gallium-Indium Microspheres to the Nanoscale. *Nano Lett.* **2011**, *11*, 5104−5110.
(44) Ferris, J. H.; Kushmerick, J. G.; Johnson, J. A.; Yoshikawa Youngquist, M. G.; Kessinger, R. B.; Kingsbury, H. F.; Weiss, P. S. Design, Operation, and Housing of an Ultrastable, Low Temperature, Ultrahigh Vacuum Scanning Tunneling Microscope. *Rev. Sci. Instrum.* **1998**, *69*, 2691−2695.
(45) Dragomiretskiy, K.; Zosso, D. Variational Mode Decomposition. *IEEE Trans. Sig. Process* **2014**, *62*, 531−544.
(46) Dragomiretskiy, K.; Zosso, D. Two-Dimensional Variational Mode Decomposition. In *Energy Minimization Methods in Computer Vision and Pattern Recognition. Lecture Notes in Computer Science*; Tai, X.-C., Bae, E., Chan, T. F., Lysaker, M., Tai, X.-C., Bae, E., Chan, T. F., Lysaker, M., Eds.; Springer International Publishing: Hong Kong, China, 2015; pp 197−208.
(47) Huang, N. E.; Shen, Z.; Long, S. R.; Wu, M. C.; Shih, H. H.; Zheng, Q.; Yen, N.-C.; Tung, C. C.; Liu, H. H. The Empirical Mode Decomposition and the Hilbert Spectrum for Nonlinear and Non-Stationary Time Series Analysis. *Proc. R. Soc. London, Ser. A* **1998**, *454*, 903−995.
(48) Jian, J.; Jian, A. Displacement Measurement and Its Application in Interframe Image Coding. *IRE Trans. Commun. Syst.* **1981**, *29*, 1799−1808.
(49) Love, N. S.; Kamath, C. An Empirical Study of Block Matching Techniques for the Detection of Moving Objects. *Proc. SPIE* **2006**, 1−36.
(50) Saavedra, H. M.; Thompson, C. M.; Hohman, J. N.; Crespi, V. H.; Weiss, P. S. Reversible Lability by *in Situ* Reaction of Self-Assembled Monolayers. *J. Am. Chem. Soc.* **2009**, *131*, 2252−2259.
(51) Andrews, A. M.; Liao, W.-S.; Weiss, P. S. Double-Sided Opportunities Using Chemical Lift-Off Lithography. *Acc. Chem. Res.* **2016**, *49*, ASAP and in press. DOI: 10.1021/acs.accounts.6b00034.
(52) Poirier, G. E. Characterization of Organosulfur Molecular Monolayers on Au{111} using Scanning Tunneling Microscopy. *Chem. Rev.* **1997**, *97*, 1117−1128.
(53) Han, P.; Mantooth, B. A.; Sykes, E. C. H.; Donhauser, Z. J.; Weiss, P. S. Benzene on Au{111} at 4 K: Monolayer Growth and Tip-Induced Molecular Cascades. *J. Am. Chem. Soc.* **2004**, *126*, 10787−10793.

DOI: 10.1021/acsnano.6b01717
ACS Nano 2016, 10, 5446−5451